AN INVESTIGATION OF THE EFFECT OF A LAMINAR BODY BOUNDARY LAYER ON THE BODY INTERFERENCE PRESSURES OF A WING-BODY COMBINATION AT MACH NUMBER 1.9

T. R. Rhees
and
W. P. Crenshaw

AN INVESTIGATION OF THE EFFECT OF A LAMINAR BODY BOUNDARY LAYER ON THE BODY INTERFERENCE PRESSURES OF A WING-BODY COMBINATION AT MACH NUMBER 1.9

by

LCDR T. R. RHEES, USN

LT W. P. CRENSHAW, USN

May, 1954

AN INVESTIGATION OF THE EFFECT OF A LAMINAR BODY BOUNDARY LAYER ON THE BODY INTERFERENCE PRESSURES OF A WING-BODY COMBINATION AT MACH NUMBER 1.9

SUMMARY

Interference pressure distribution data were obtained for the body of a wing body combination with a laminar boundary layer on the body at Mach number 1.9. The model was a rectangular wing mounted on a cylindrical body. The body was maintained at zero angle of attack and the wing positioned at $\pm 8.2°$ angle of attack.

The experimental results are compared with the linearized theory of NACA TN 2677 and earlier experimental results for the same model with a turbulent boundary layer on the body.

The experimental results agree well with theory except for viscous effects not predicted by linear non-viscous theory. In comparison with the turbulent case the laminar boundary layer on the body with negative wing angle of attack resulted in (1) local separation of the laminar boundary layer, with a plateau of slightly increased pressure ahead of the shock pressure rise (2) greater upstream propagation of the pressure disturbance both in terms of boundary layer thicknesses and actual distance (3) overshooting of the shock pressure rise. The type of boundary layer on the body did not have an appreciable effect with the wing at positive angle of attack.

In Appendix A it is concluded that prediction of body lift force due to the wing-body interference by the method of NACA TN 2677 will be conservative for the two possible configurations considered.

SYMBOLS

C_p = pressure coefficient, $\frac{p - p_1}{\frac{\rho_1}{2} V_1^2}$

M_1 = free-stream Mach Number

p = static pressure at any particular body orifice, lb/sq in.

p_1 = static pressure at any particular body orifice, body alone, lb/sq in.

R = radius of cylindrical body, inches

Re_x = Reynold's Number, based on length from nose

V_1 = free-stream velocity, ft/sec.

X = distance from leading edge of wing, inches

x = axial distance from nose, inches

α_B = body angle of attack, zero in all cases

α_W = angle of attack of the wing

$\beta = \sqrt{M_1^2 - 1}$

δ = body boundary layer thickness, inches

θ = angle between meridional plane under consideration and the horizontal plane, deg.

ρ_1 = free-stream density, slugs/cu ft.

AN INVESTIGATION OF THE EFFECT OF A LAMINAR BODY BOUNDARY LAYER ON THE BODY INTERFERENCE PRESSURES OF A WING-BODY COMBINATION AT MACH NUMBER 1.9

INTRODUCTION

This investigation was conducted to obtain quantitative information as to the effect of a laminar body boundary layer on the pressure distribution on a body due to the presence of a wing in a supersonic flow. In addition, it was desired to compare this laminar body boundary layer incremental pressure distribution with the theoretical inviscid flow solution and a similar experimental pressure distribution for a turbulent body boundary layer.

The method of Nielsen, Ref. 1, permits theoretical solutions of the linearized wing-body interaction equations for inviscid flow.

For the particular wing-body combination used in this investigation, the theoretical inviscid pressure profiles and experimental pressure profiles measured for a turbulent boundary layer on the body are presented in Refs. 2 and 3. The present investigation extends this experimental work and permits comparison between the two viscous flow cases, laminar and turbulent boundary layer on the body.

In general there are two effects of shock-wave-boundary layer interaction: (1) the presence of subsonic velocities in the

boundary layer permits propagation of pressure disturbances within the subsonic portion of the boundary layer, thus influencing the flow field ahead of the Mach cone whose apex is at the disturbance; (2) the sharp pressure gradients which may exist in a supersonic stream can induce sizeable cross flows in the boundary layer or even separation of the boundary layer.

This investigation was conducted by LCDR Thomas R. Rhees, USN, and LT William P. Crenshaw, USN, during February, 1954, at the Supersonic Wind Tunnel, University of Michigan, Ann Arbor, Michigan, as part of the third-year curriculum in Aeronautical Engineering of the U. S. Naval Postgraduate School, Monterey, California. The project was financed by the Bureau of Aeronautics, Navy Department, Washington, D. C.

The authors are especially indebted to Dr. H. E. Bailey, Research Associate, Engineering Research Institute, for invaluable assistance and guidance in the conduct of the investigation.

EQUIPMENT AND PROCEDURE

Experimental work was performed in the University of Michigan 8 by 13-inch Supersonic Wind Tunnel, Mach 1.9 channel. A complete description of this facility is contained in Ref. 4.

Description of Model.

The model, Figs. 1 and 2, consists of a cylindrical body and two half-wings. A typical test configuration is shown in Fig. 3. The body is hollow, with a 2-inch outer diameter and a 1-1/2-inch inner diameter. The nosepiece is 2.55-inches long and tapers to an inlet

diameter of 1-5/16-inches. The model is identical with that used in Ref. 3 except for use of a shorter nose-piece which insures a laminar flow in the boundary layer on the body in the test region. This permits a direct quantitative comparison between the results obtained for the turbulent and laminar boundary-layers.

The body is hollow to keep the nose shock as weak as possible and at the same time keep the model length short enough to insure a laminar body boundary layer in the region of interest.

The flat spots on the sides of the body where the wings meet the body are necessary to prevent a gap between wing and body when the wing is at some angle of incidence with respect to the body. The effects of these flat spots are negligible so far as could be determined from the pressure readings on the body.

The support strut is sufficiently far downstream from the orifice region so that pressure disturbances caused by the strut do not affect the orifice region.

The body was at zero angle of attack with respect to the free stream for all runs.

The axial position of the body may be varied about 1-1/2-inches by axial movement of the strut attachment bolting to the top of the Wind Tunnel, Fig. 2. The axial position of the body was determined with respect to the leading edge of the wing within $\pm$.003 inch. Since the wings are fixed with respect to the wind tunnel, this axial body movement permits the measurement of pressure profiles on the body due to the wing.

The body contains 92 pressure orifices, which lie in planes

inclined at an angle of 40° with respect to the body axis and are 1/2-inch apart. The orifices also lie in the meridional planes $\theta = 0°, \pm 5°, \pm 10°, \pm 15°, \pm 20°, \pm 30°, \pm 40°, \pm 50°, \pm 60°, \pm 75°, \pm 90°$. Each meridional plane has orifices in alternating inclined planes. In the present investigation 44 of the orifices were used, in the upper quadrant, as shown in Fig. 1, including only the leading orifice in the $\theta = 0°$ plane.

The two half-wings are supported by brackets outside the test section, as shown in Fig. 3. The sealing of the wing-body juncture was accomplished by mechanical contact, with a maximum gap slightly greater than .008-inch at the leading edge of the wing.

The chord of the wing is 2-inches and the half-span is 2-1/2 inches. The wing section is flat on one side and double-wedge shaped on the other side, with a wedge angle at the leading edge of 10°. The wings were mounted at angles of attack $\pm 8.2°$ with the flat side of the wing nearest the pressure orifice on the body. The variation of angle of attack setting for all runs was negligible.

Instrumentation.

The static pressures were measured with mercury manometers, which were photographed during the test run, permitting an accuracy in the measurements of 1% of the ambient static pressure.

Schlieren photographs of each configuration were obtained, and are shown in Figs. 6 and 7. Although the body and wing support brackets obscure the most interesting portion of the schlieren field, the approximate thickness of body boundary layer in the meridional planes $\theta = \pm 90°$ can be obtained.

The china-clay technique was used to illustrate the flow in the boundary layer close to the surface of the body, Figs. 8 and 9. The china-clay pattern was especially useful in locating the traces of shock-waves on the model surface.

Experimental Procedure.

Prior to taking data two runs were made: (1) Visual schlieren observation showed nose shock attached and no blocking. (2) China-clay pattern indicated laminar body boundary layer forward of wing leading edge Mach helix.

Pressure data were obtained for $\pm 8.2°$ wing angle of attack, with body angle of attack zero, and also for the body alone at zero angle of attack. The china-clay pattern was checked on every run to insure that the laminar body boundary layer was maintained. Pressure readings in three meridional planes were plotted after each run to check immediately the reliability of the pressure data for that run.

Data Preparation.

Non-uniformities in the tunnel flow field, though small, introduce some errors in the pressure readings.

The pressure on the body alone measured at any one orifice may be written

$$p_{measured} = p_{body\ alone} + \Delta p_{induced},$$

where $p_{body\ alone}$ is the pressure on the body alone in a uniform flow and is a function only of the geometry of the particular body, and $\Delta p_{induced}$ is the incremental pressure induced on the body alone due to the wind-tunnel flow non-uniformities and is a function of body geometry and the wind-tunnel flow non-uniformities.

If the wing is introduced into the flow the measured pressure becomes

$$p_{measured} = p_{body\ alone} + \Delta p'_{induced} + \Delta p_{interference},$$

where $p_{body\ alone}$ is as defined above, $\Delta p'_{induced}$ is the incremental pressure induced on the body in the presence of the wing due to the wind-tunnel non-uniformities and $\Delta p_{interference}$ is the incremental pressure induced on the body in a uniform flow due to the presence of the wing. Uniform flow is the condition usually encountered in free flight but extremely difficult to obtain in a wind tunnel.

Provided $\Delta p_{interference}$, $\Delta p_{induced}$ and $\Delta p'_{induced}$ are small quantities,

$$\Delta p_{induced} = \Delta p'_{induced},$$

so that a simple subtraction of the pressures on the body alone from the pressures on the body in the presence of the wing gives $\Delta p_{interference}$, which is the desired result.

Fig. 4 shows the raw experimental data obtained from the row of orifices in the meridional plane $\theta = 30°$ for the body alone as well as the body plus the wing at -8.2° angle of attack. The bump in the body alone pressure curve indicates that a weak shock wave strikes the body just upstream of the wing trailing-edge. A similar bump occurs on the pressure curve of the body in the presence of the wing, but it is shifted upstream. This axial shift is due to the fact that the tunnel shock bends forward after intersecting the shock-wave from the wing leading-edge, i.e., there is some interaction between

$\Delta p_{induced}$ and $\Delta p_{interference}$.

The experimental pressure profiles in this report were obtained from the difference between the faired pressure curves for the body alone and for the body in the presence of the wing in order to eliminate as far as possible the effect of tunnel flow non-uniformities.

The curves presented herein for the various configurations are plots of $\beta C_p/\alpha_w$. The zero base for all curves is the static pressure measured on the body alone. It should be noted that, although the curves are in effect non-dimensionalized for presentation, they apply strictly only for $\alpha_w = \pm 8.2°$. Refs. 3 and 6 observed that the interference pressure distribution is affected by the angle of attack of the wing.

RESULTS AND DISCUSSION

In Figs. 6 and 7 the nose shock is seen impinging on the side window as a curved irregular line. The reflection of this nose shock from the side walls strikes the body between the last two inclined rows of orifices. This reflected shock affected the pressure measurements of the final row of orifices and those measurements were not utilized in preparing the pressure curves. The reflection from the tunnel top and bottom struck the body downstream of the orifice region.

From the schlieren photograph of the body alone, Fig. 6, the measured laminar body boundary-layer thickness at a point 8 inches aft of the nose is 0.03 inch. From Ref. 7, the compressible laminar

boundary-layer thickness on a flat-plate is

$$\delta = \left[5.2 + 1.03(\gamma - 1)M_1^2\right] \frac{x}{R_{e_x}^{1/2}}.$$

For a Reynold's Number of 2.8×10^6, the calculated boundary-layer thickness is 0.032 inch, which is in good agreement with the measured value.

The experimental interference pressure distributions on the body with a laminar boundary layer in the presence of the wing at $\alpha_w = \pm 8.2°$ are plotted in Fig. 10 as solid lines. The theoretical and turbulent boundary-layer interference pressure distributions from Refs. 2 and 3 are plotted in Fig. 10 as dashed lines.

Composite plots of the interference pressure distribution with laminar body boundary layer in several meridional planes are plotted in Fig. 11 for $\alpha_w = \pm 8.2°$.

Data for the meridional planes $\theta = 0°$ and $\theta = 5°$ are incomplete since some of the orifices in these planes are covered by the wing. These data are therefore not presented.

For a non-zero wing angle of attack there is a foreshortening effect which modifies the body area between the Mach helices from the wing leading- and trailing-edge junctures compared with the linearized helices, see Fig. 5. For $\alpha_w = \pm 8.2$ each helix is shifted axially by an amount $X/\beta R = 0.15$.

Wing at Negative Angle of Attack, $\alpha_w = -8.2°$.

For negative wing angles of attack, a compression occurs over the flat surface of the wing. In an ideal fluid, the pressure

coefficient on the body is zero ahead of the Mach helix generated at the wing-body juncture; the pressure rise at the helix is a discontinuous shock jump followed by a continuous axial pressure gradient due to the interference potential field. The magnitude of the shock jump is continuously attenuated as the shock moves around the cylinder, diminishing to zero at the top meridian. In an actual fluid, however, the presence of a boundary layer on the body permits upstream propagation of the pressure rise due to this wing leading-edge shock. For a boundary-layer thickness of 0.03 inch, and with the foreshortening effects of α_w taken into account, Fig. 10 indicates that the upstream propagation varies from about 30 boundary-layer thicknesses in the plane $\theta = 10°$ to about 60 boundary-layer thicknesses in the $\theta = 90°$ plane. Comparison with the curves from Ref. 3, (Fig. 10) shows that the upstream propagation in terms of boundary-layer thicknesses is 7 to 10 times that observed for the turbulent boundary-layer. The upstream propagation apparently terminates near the limit of the orifice region in the forward position. In the absence of reliable check data in this area the curves of Fig. 10 were terminated short of the most forward data points and are conservative in their indication of upstream propagation of the pressure disturbance. The magnitude of this forward propagation in the laminar boundary-layer is in general agreement with the flat-plate shock-boundary layer results of Ref. 5.

The profiles of Fig. 10 have a plateau of fairly constant pressure, indicating a region of flow separation, which increases toward the top of the body. Fig. 9 shows a large area of probable

separation where the china clay is still wet, ahead of the Mach helix. The variation in the amount of upstream propagation with θ is due in part to the cross flow of the low inertia air in the boundary layer on the body which results in an accumulation of air along the top meridional plane. This cross flow (see Fig. 9) is produced by the component of the shock induced velocity which is normal to the free stream direction. The cross-flow component in the laminar boundary layer appears considerably stronger than that shown in the china-clay photographs of Ref. 3 for the turbulent boundary layer with approximately the same wing angle of attack. Considering planes of constant $X/\beta R$, Fig. 11 shows the strong lateral pressure gradient which causes this cross flow.

The maximum experimental value of $\beta C_p/\alpha_w$ agrees well with theory. In all meridian planes it is higher than the theoretical maximum. The laminar boundary layer curves of Fig. 10 are considerably higher than the curves for the turbulent boundary layer, which agrees with the results of Refs. 5 and 6. At low values of θ the shock pressure rise occurs at about the theoretical position, considering the foreshortening effect, but moves forward of the theoretical curve at the higher meridians. This is due in part to the crossflow in the boundary layer and in part to the change in the wave angle which results when a Mach wave is used to approximate a shock wave.

The viscous effects result in a pronounced smoothing out of the pressure rise due to the shock, although the smoothing out is not as great as for the case of turbulent boundary layer on the body.

The slope of the pressure curves decreases with increasing θ until about $\theta = 75°$, above which the pressure augmentation from the opposite wing increases both the maximum pressure and the slope. The main pressure rise for the laminar boundary layer occurs later than for the turbulent boundary layer and tends to overshoot at low values of θ, which is in general agreement with Ref. 5. The pressure profiles are very similar to those obtained in Ref. 6 for a comparable case, except that nonlinear effects are more pronounced here due to the larger wing angle of attack considered.

The trailing-edge expansion occurs slightly ahead of the theoretical pressure drop, foreshortening considered, but agrees well with turbulent results at low values of θ. As in the turbulent case, the trailing-edge expansion for $\theta < 20°$ is actually greater than the compression due to the leading-edge shock, so that the pressure curves overshoot the ambient pressure and then begin to approach it assymptotically from below. The pressure behavior downstream of this point is uncertain due to flow non-uniformities and body nose shock effects.

Wing at Positive Angle of Attack, $\alpha_w = +8.2°$.

For positive angles of attack, an expansion wave originates at the leading edge of the wing. As seen in Fig. 10, this expansion wave is preceded at small values of θ ($\theta < 40°$) by a slight compression, probably a continuation of the strong shock wave on the compression side of the wing which is detached at the wing leading edge due to the finite thickness thereof. The compression observed is appreciably less pronounced than that obtained for the turbulent

case. This is probably due to the ability of pressure disturbances to propagate further in the laminar boundary layer. The continuation of the strong shock wave around the leading edge extends further toward the top meridian and the pressure gradient extends over a greater axial distance in the laminar boundary layer. Interaction between the shock and the boundary layer at the leading-edge of the wing-body juncture is a highly complicated viscous compressible flow phenomenon so that the picture suggested above cannot be expected to be exact in all details.

The upstream propagation of the pressure disturbance varies from about 20 boundary-layer thicknesses in the plane $\theta = 10°$ to about 30 boundary-layer thicknesses in the plane $\theta = 90°$. This is again several times that observed with the turbulent boundary layer, but less than the upstream propagation observed for the laminar boundary layer with a negative wing angle of attack.

At low values of θ, the expansion in the laminar boundary layer is seen (Fig. 10) to begin slightly ahead of that for the turbulent boundary layer, but with a lesser pressure gradient and a lower maximum expansion pressure coefficient. This maximum pressure coefficient is also appreciably lower than the theoretical value for all θ. For $\theta > 30°$, the main pressure rise occurs slightly later than that for the turbulent boundary-layer, as was noted for the wing at negative angles of attack. There is very little difference in the pressure profiles for the two boundary-layer cases for $\theta > 30°$. For the laminar boundary layer, the expansion pressure gradient at

$\theta = 10°$ is almost as steep as that of the compression shock occurring for negative angles of attack. However, for $\theta > 10°$, the fan-like nature of the expansion wave causes the pressure drop to occur over an increasing axial distance with increase in θ. In the plane $\theta = 90°$, the pressure drop is quite gentle and is spread out over an axial distance of $X/\beta R = 1.8$. The pressure gradient on the body at constant $X/\beta R$ (see Fig. 11) tends to induce crossflow in the boundary-layer from the top meridional plane towards the wing. This also is evident in the china-clay pattern of Fig. 8.

The wide difference in the maximum pressure coefficients for the wing at positive and the wing at negative angle of attack is due to the marked difference in viscous effects associated with the interaction of an expansion wave or a shock wave with a laminar boundary layer. Similar effects were observed in Ref. 6.

CONCLUSIONS

The boundary layer on the body permits upstream propagation on the body of the pressure disturbances from the wing in a supersonic flow. These disturbances cause a strong cross flow in the boundary layer which results in a variable amount of upstream propagation of the pressure disturbances.

For the case of a shock-wave at the leading edge of the wing flow separation occurs on the body ahead of the trace of the shock on the body, resulting in a region of fairly constant but slightly increased pressure. The size of this separated flow region increases markedly toward the top meridian of the body.

With a shock at the leading edge the experimental results up to the trailing edge agree well with theory if the linear theory is corrected to the position indicated by simple shock-wave theory. Beyond the trailing edge the theory is no longer applicable. For the meridional planes near the flat surface of the wing the initial sharp pressure rise overshoots the theoretical curve.

With an expansion at the leading edge of the wing the experimental results are low compared with theory.

The pressure disturbances propagate further upstream for a laminar boundary layer both in terms of boundary layer thicknesses and in terms of actual distances than for a turbulent boundary layer on the body. The main pressure rise for a leading-edge compression occurs later and the maximum pressure is considerably greater for the laminar case than for the turbulent case. For an expansion at the leading edge the main pressure decrease occurs later for a laminar than for a turbulent boundary layer on the body. The minimum pressure in both cases is about the same. Thus the type of boundary layer on the body does not have as great an effect on the interference pressure distribution for positive angle of attack of the wing as for negative angle of attack.

The china-clay pattern of Fig. 8 shows that the wing trailing-edge shock deflects the boundary-layer flow back to approximately the free-stream direction. The flow on the body aft of a point about 1 inch behind the wing trailing-edge is influenced by the strong disturbance originating at the outboard wing-tip.

APPENDIX A

LIFT FORCE ON THE BODY DUE TO WING-BODY INTERFERENCE

The lift force on the body at zero angle of attack due to the presence of the wing at an angle of attack was obtained by integrating the body pressure profiles of Fig. 10 with a planimeter.

For the laminar boundary layer on the body, the observed body pressure data pertain to the quadrant of the body surface above the flat side of the wing, for wing angles of attack of $\pm 8.2°$. The algebraic sum of the integrated pressure components for each of the two angles of attack thus gives, in effect, the body lift force in the presence of a flat-plate wing. The theoretical and the turbulent body pressure profiles above the flat surface of the wing in Ref. 3 have been integrated, thus a quantitative comparison between the experimental and the theoretical lift forces is possible.

Since the presence of wing-tip effects and tunnel non-uniformities render the observed data inaccurate a short distance downstream of the trailing edge of the wing, this comparison was limited to the two following cases:

Case I - The body is assumed to terminate at the trailing edge of the wing. This is applicable, for example, to control surfaces at the tail of a missile.

Case II - The body is assumed to terminate at a distance of one chord-length downstream of the trailing edge of the wing.

The results for Case I are accurate within the limits of the experimental data. For Case II, the results are less accurate due to the flow irregularities noted above.

The results of the lift force integrations for the two cases are as follows:

	Case I	Case II
Theoretical	0.612 lb	2.993 lb
Laminar Boundary Layer on Body	0.644 lb	3.014 lb
Turbulent Boundary Layer on Body	0.991 lb	3.263 lb

From these results, it is concluded that prediction of the body lift force due to the wing-body interference using the method of Ref. 1 will be conservative for configurations similar to the above. Further, the theoretical value is approximated much more closely if the boundary layer on the body is laminar.

REFERENCES

1. Nielsen, J. N., and Pitts, W. C. "Wing-Body Interference at Supersonic Speeds with an Application to Combinations with Rectangular Wings." NACA TN 2677, April, 1952.

2. Bailey, H. E., and Phinney, R. E. "Final Report, Wing-Body Interference, Part I, Theoretical Investigation." University of Michigan, Engineering Research Institute, Project M937-1-F.

3. Bailey, H. E., and Phinney, R. E. "Final Report, Wing-Body Interference, Part II, Experimental Investigation." University of Michigan, Engineering Research Institute, Project M937-2-F.

4. Garby, L. C., and Nelson, W. C. "University of Michigan 8 x 13 inch Intermittent-Flow Supersonic Wind Tunnel." University of Michigan Memorandum No. 59, Engineering Research Institute, June, 1950.

5. Liepmann, H. W., Roshko, A., and Dhawan, S. "On Reflection of Shock Waves From Boundary Layers." NACA TN 2334, April, 1951.

6. Pitts, W. C., Nielsen, J. N., and Gionfriddo, G. N. "Comparison Between Theory and Experiment for Interference Pressure Field Between Wing and Body at Supersonic Speeds." NACA TN 3128, April, 1954.

7. Kuethe, A. M., and Schetzer, J. D. Foundations of Aerodynamics. John Wiley and Sons, 1950.

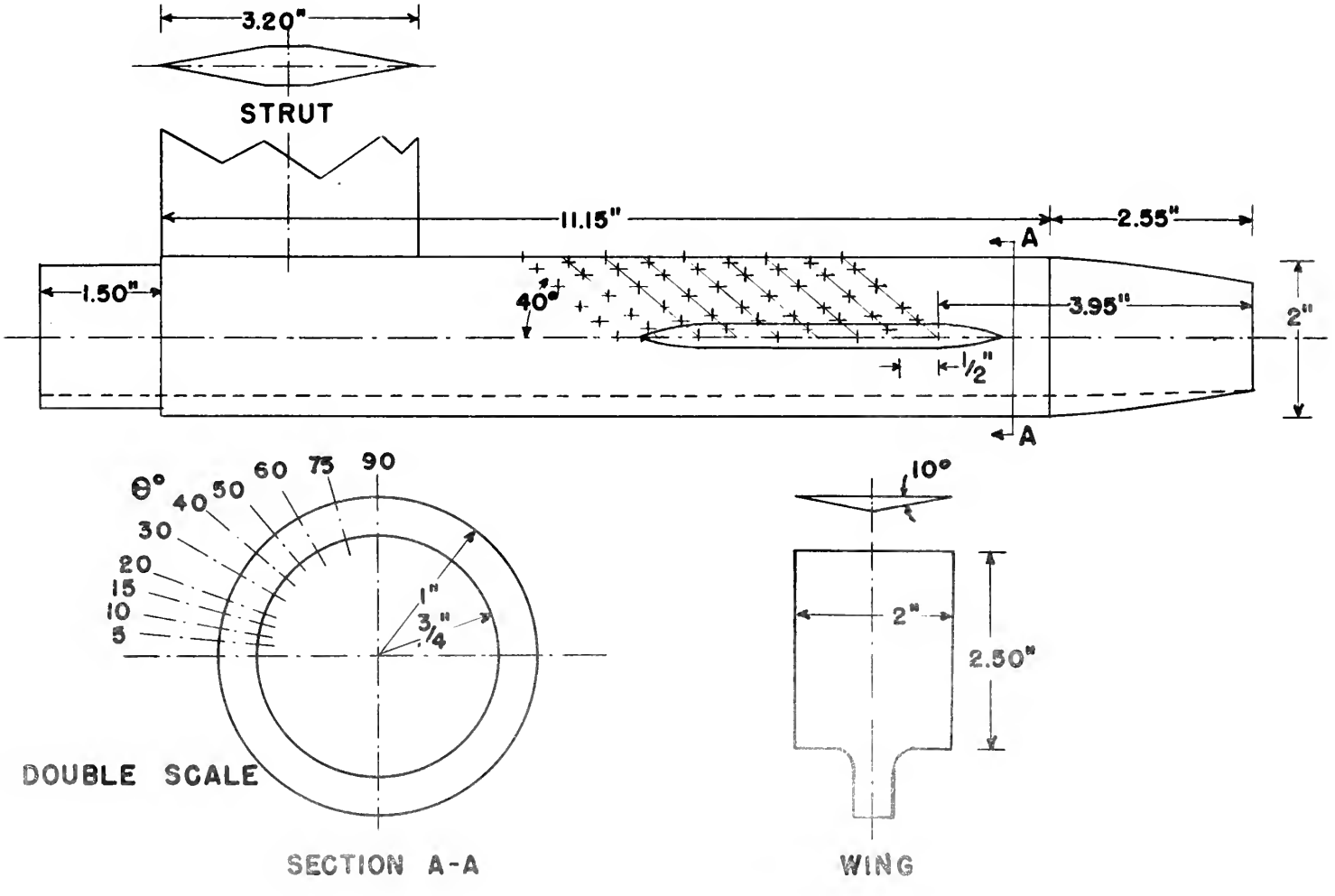
3.20"
STRUT
11.15"
2.55"
A
1.50"
40°
3.95"
2"
1/2"
A
θ°
40
50
60
75
90
30
20
15
10
5
1"
3/4"
DOUBLE SCALE
SECTION A-A
10°
2"
2.50"
WING

Fig. 1 – Model

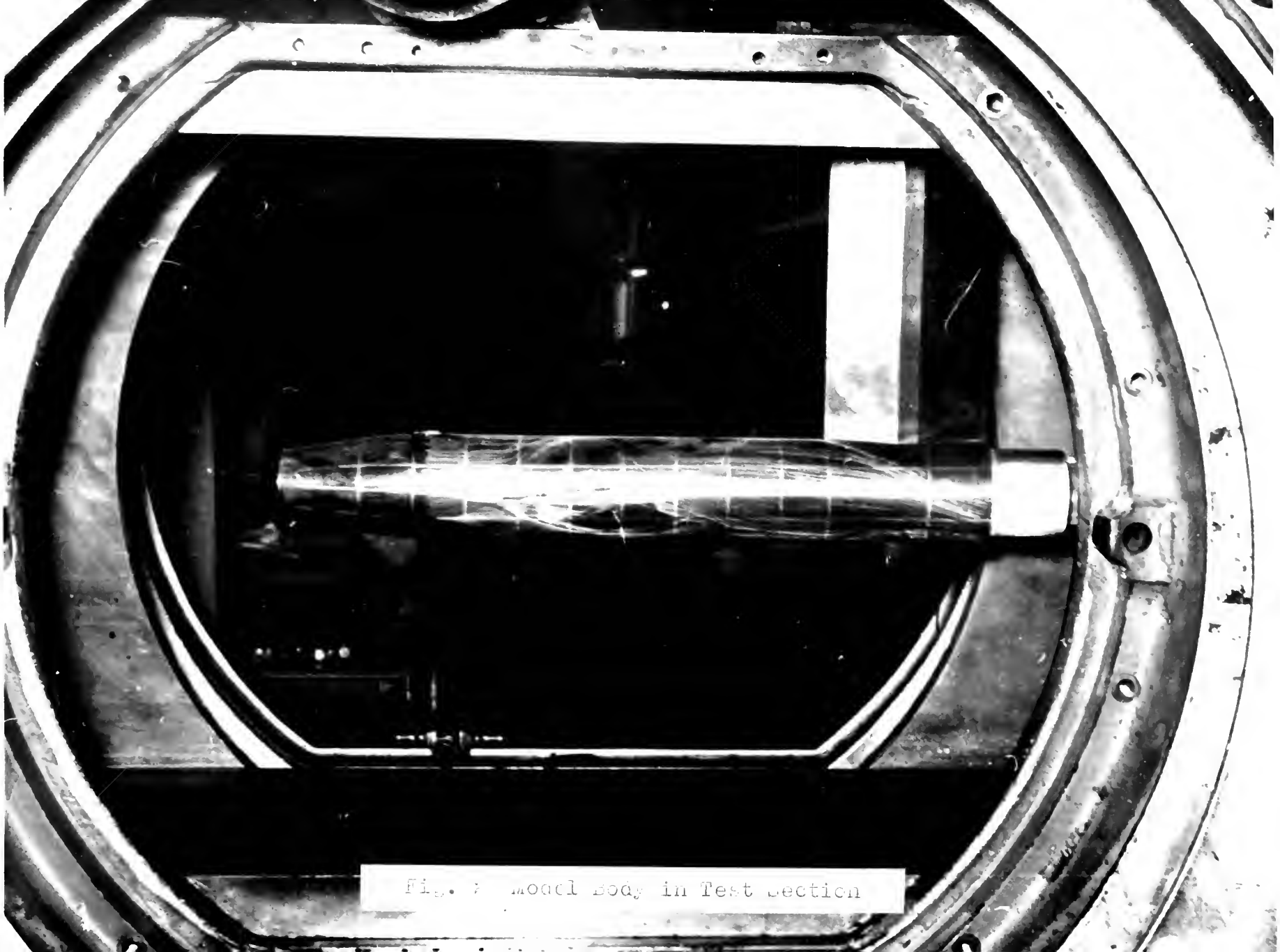

Fig. 7 Model Body in Test Section

Fig. 4 Test configuration, $\alpha_v = -5.0°$

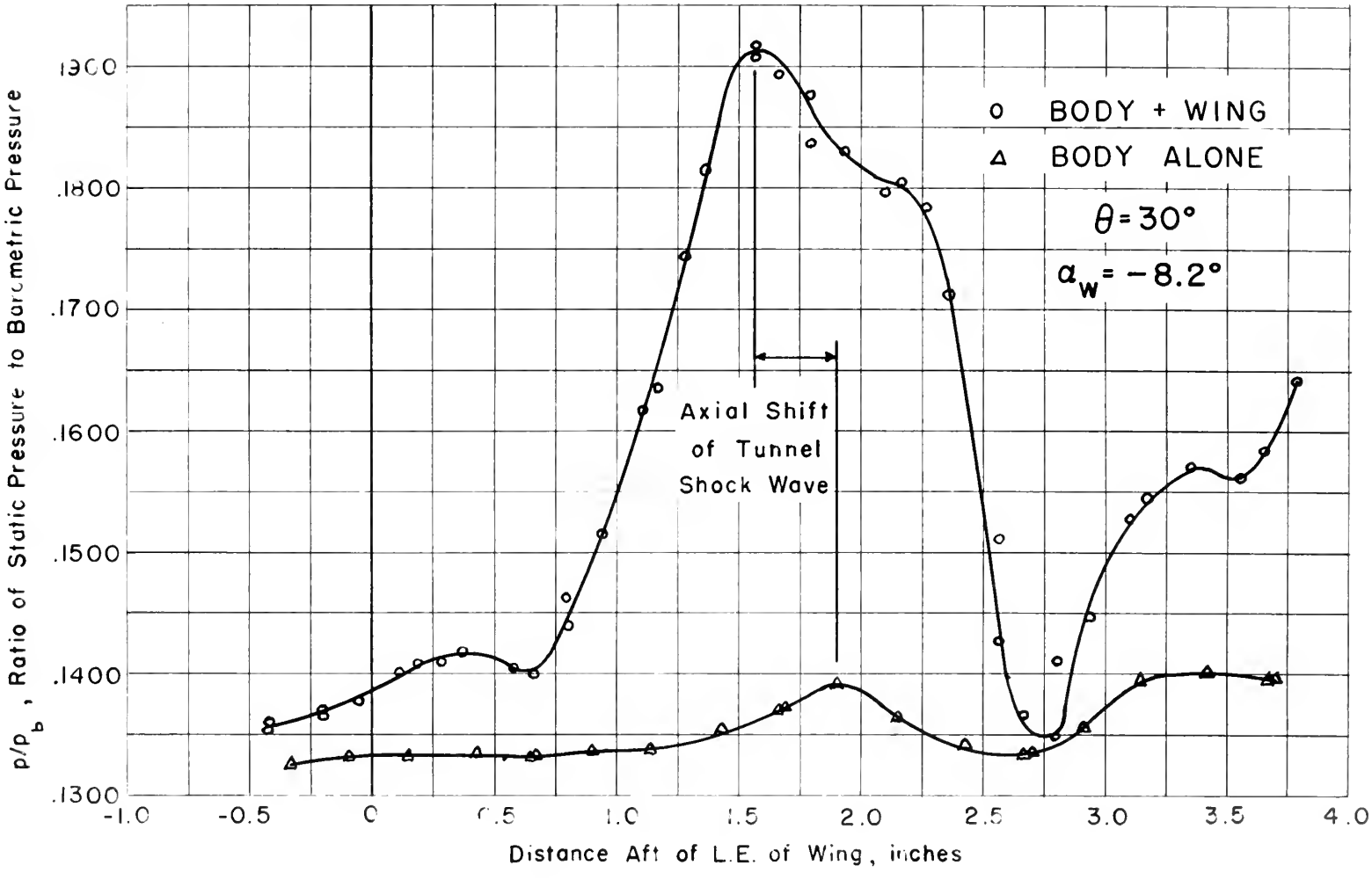

Fig. 4 Sample of Raw Experimental Data

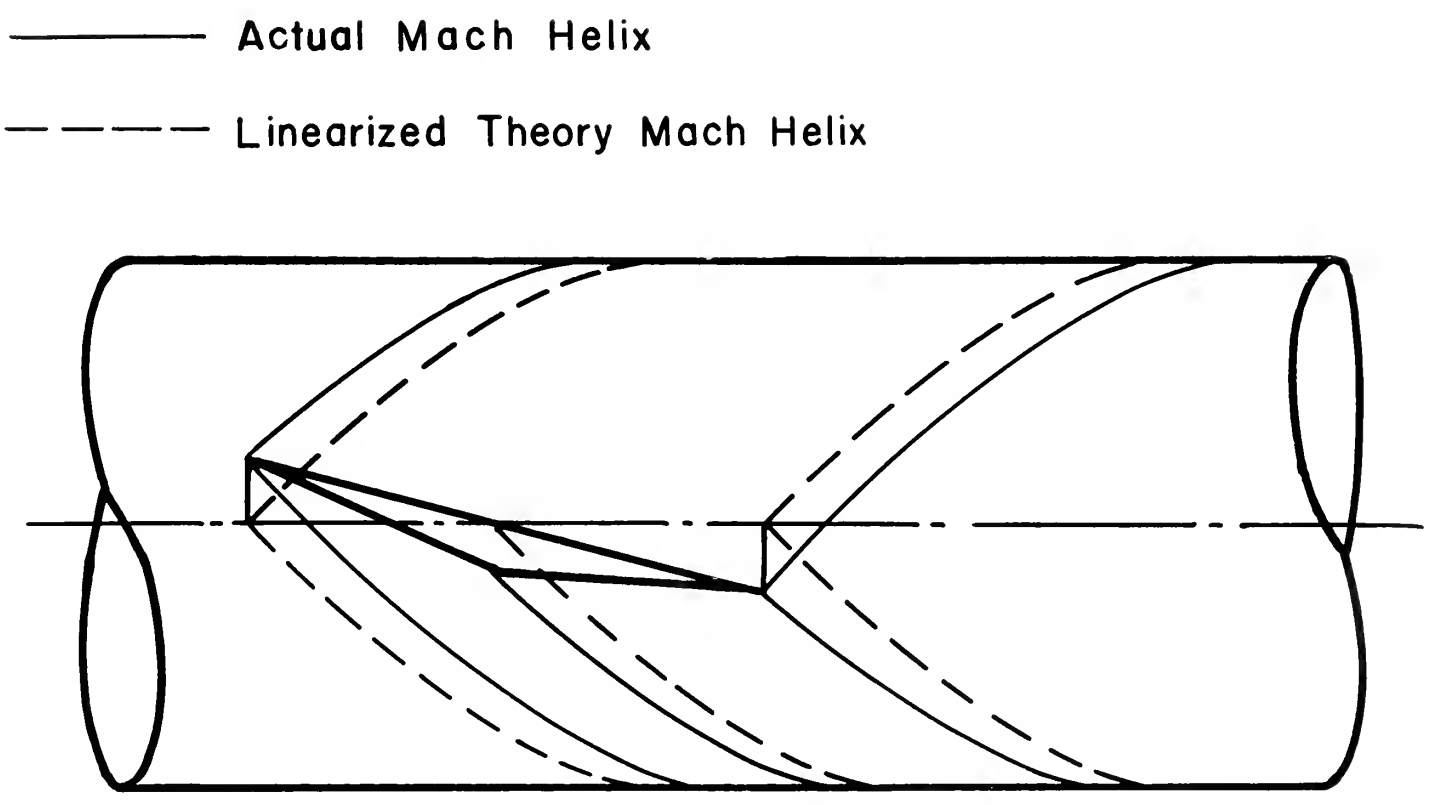

Fig. 5. Effect of Wing Incidence on the Region of the Body Influenced by the Wing.

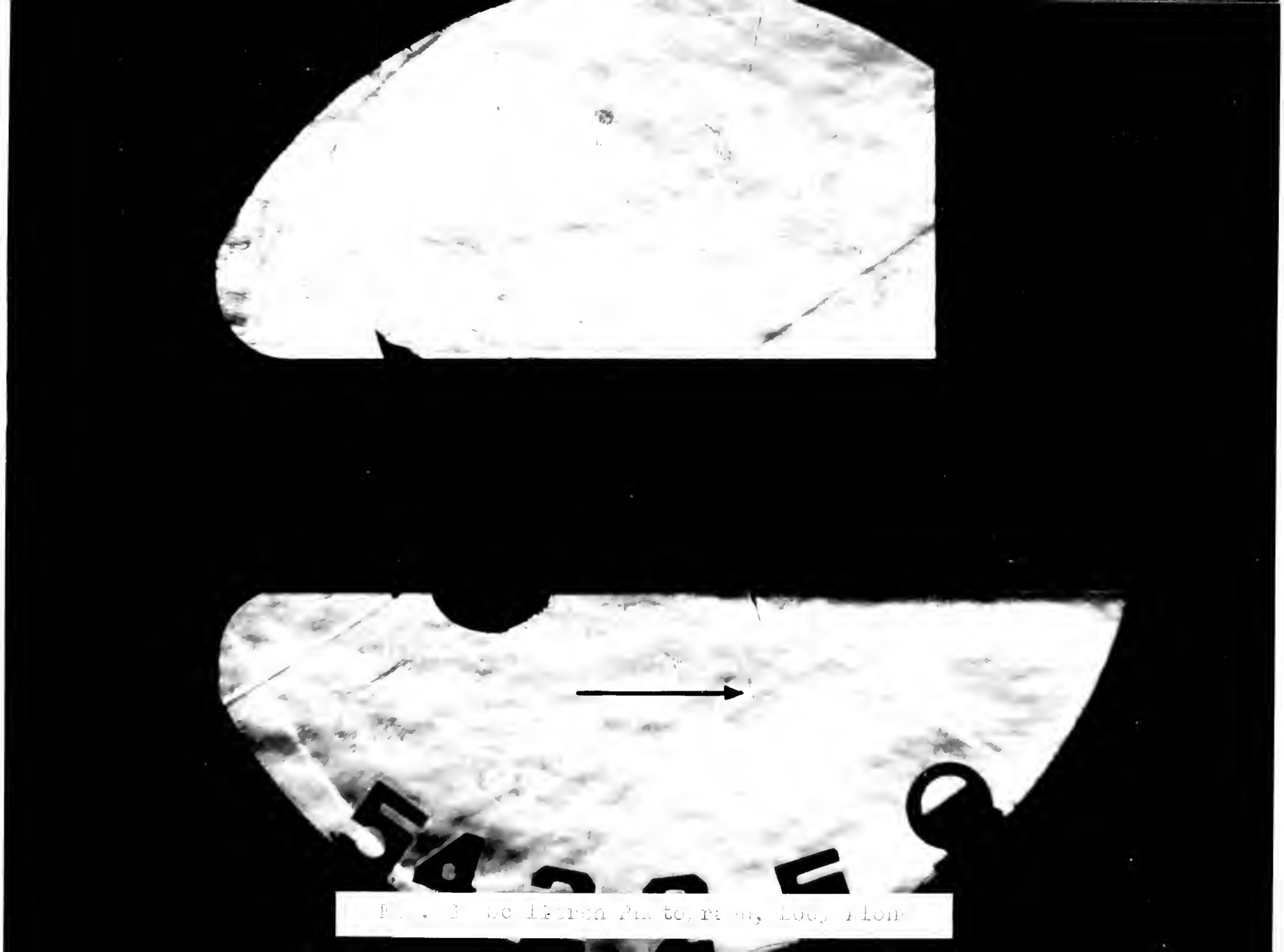

Fig. 3 Ice Lenses Photographed Looking Along

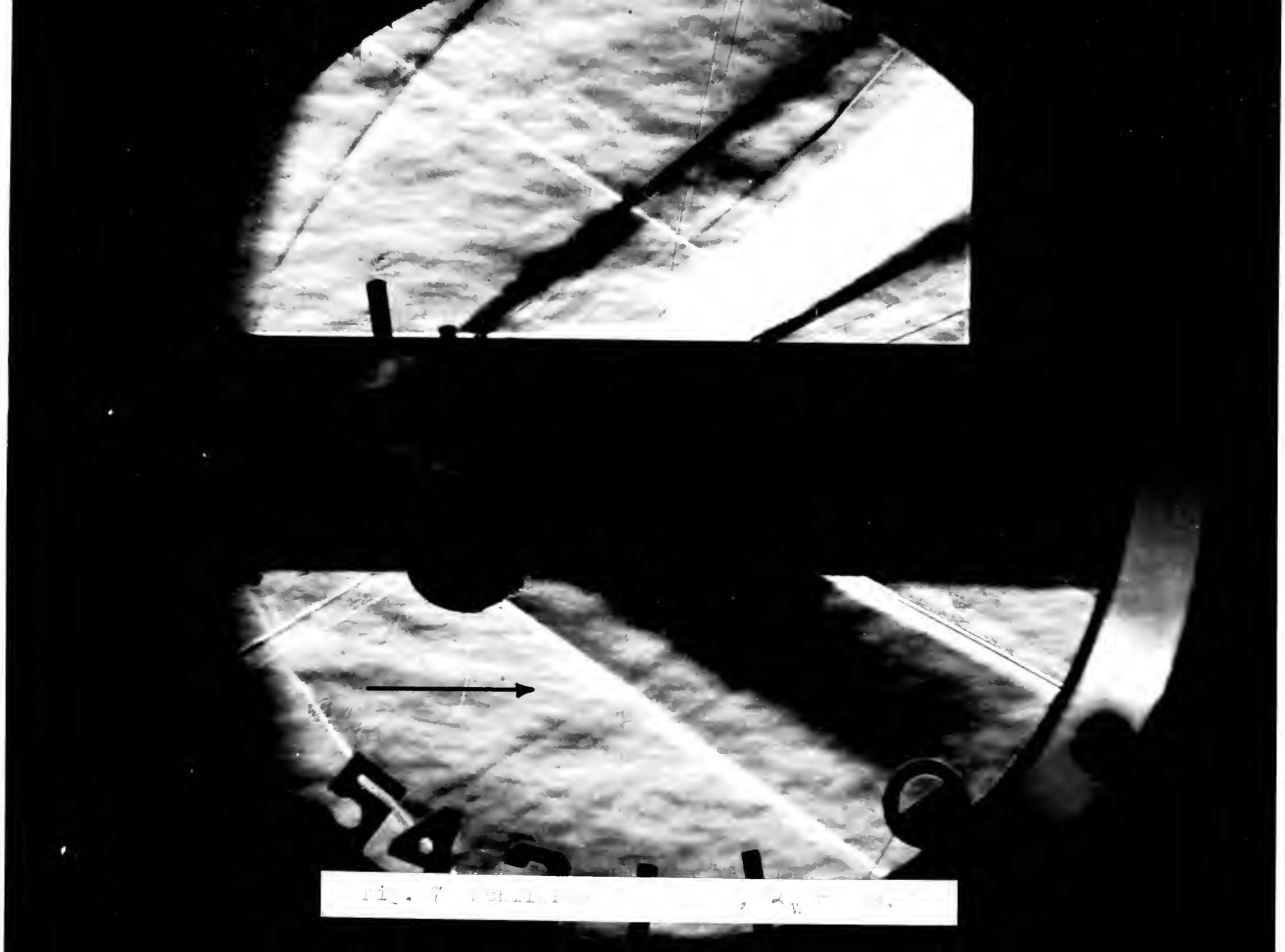

Fig. 8 China-clay Pattern, $\alpha_{V.} = + 8.5^{\circ}$

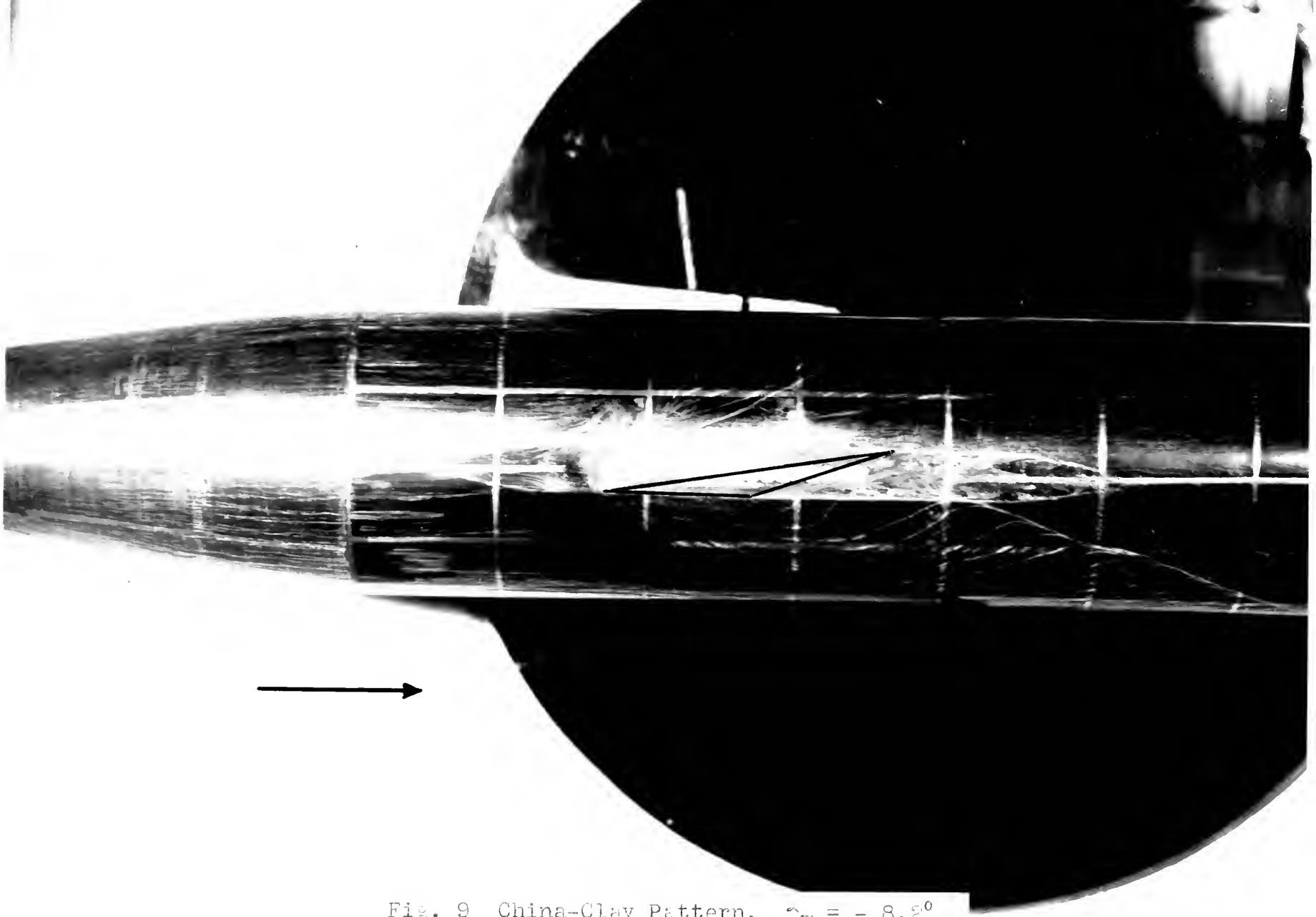

Fig. 9 China-Clay Pattern, $\alpha_W = -8.2^0$

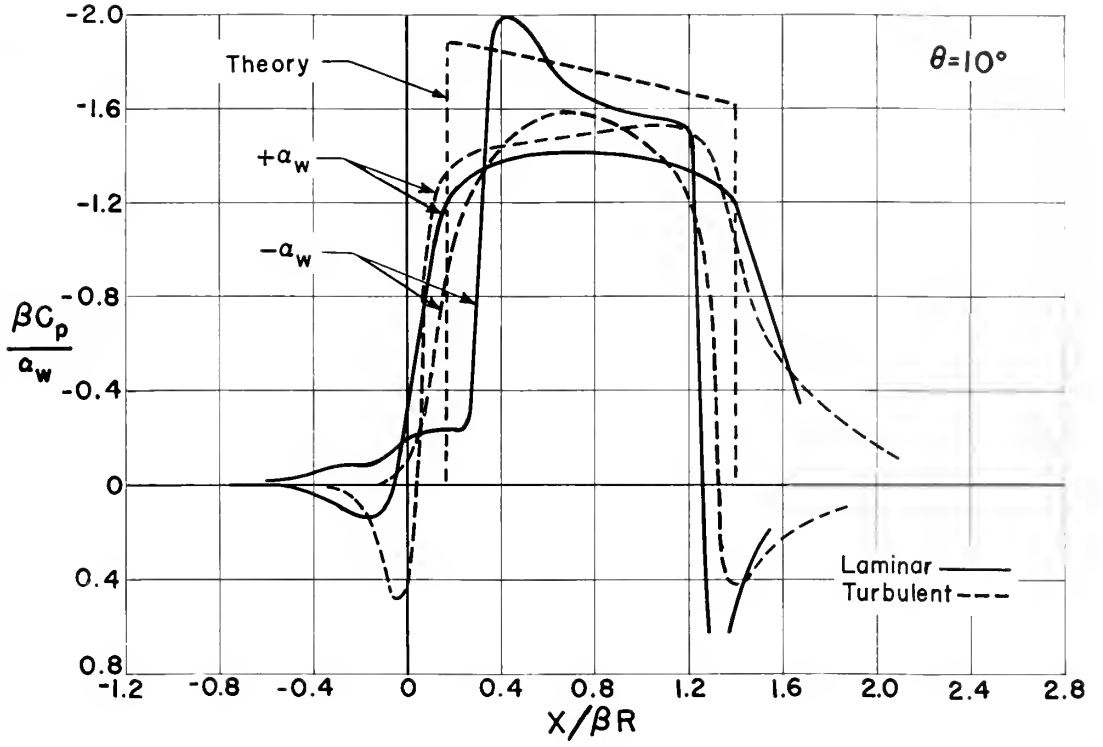

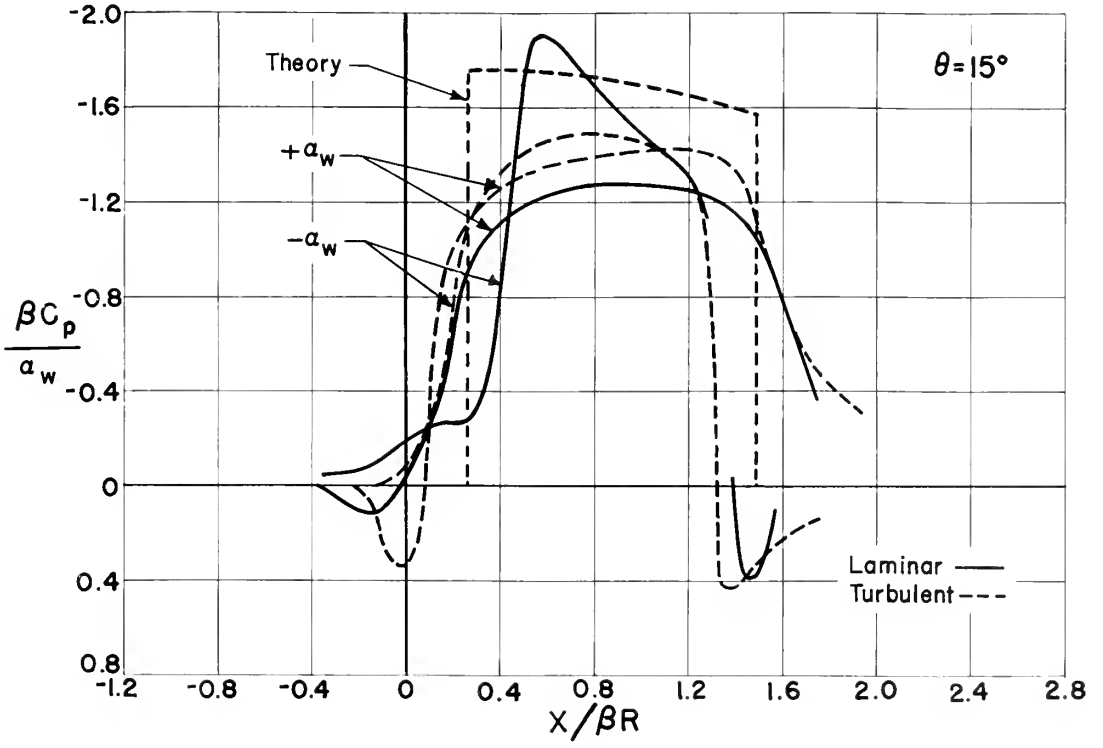

Fig. 10 Body Pressure Profiles, $\alpha_B = 0$

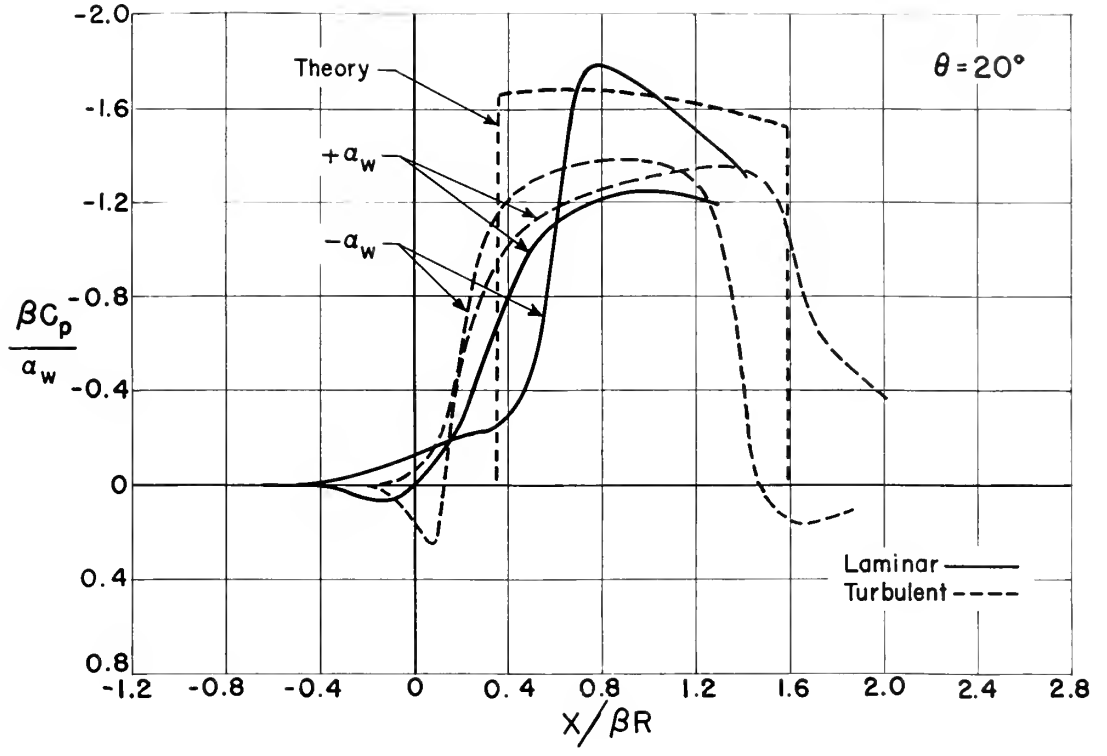

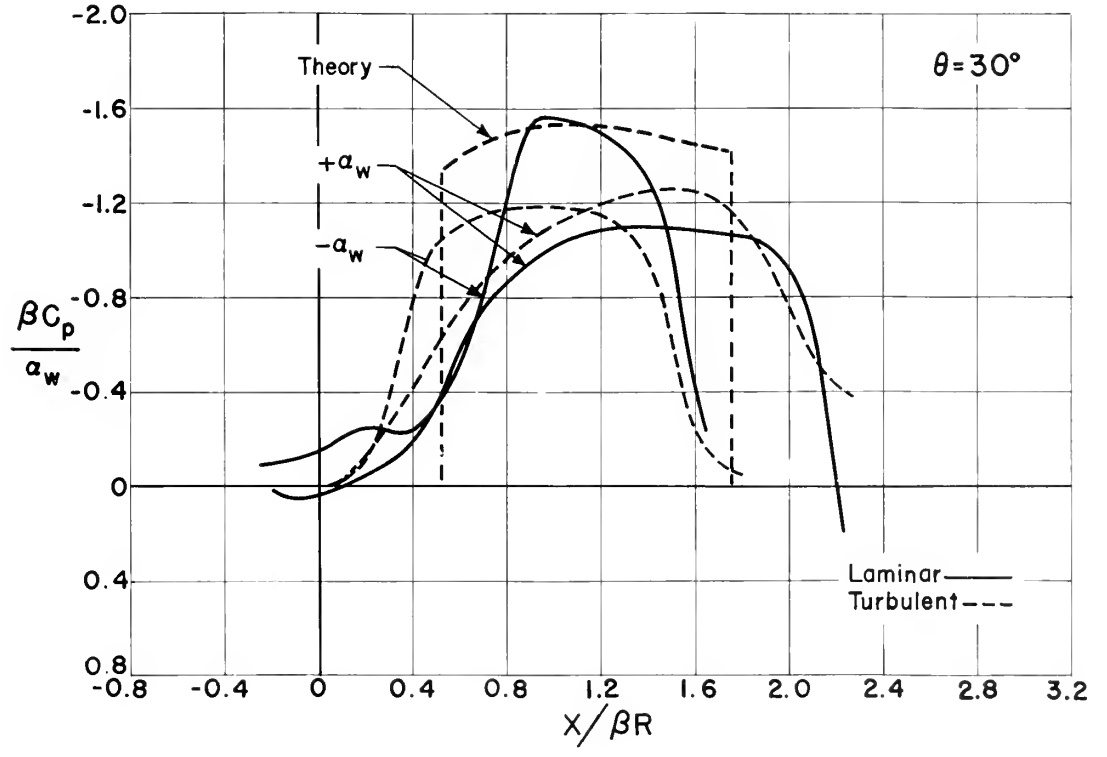

Fig. 10 (Continued)

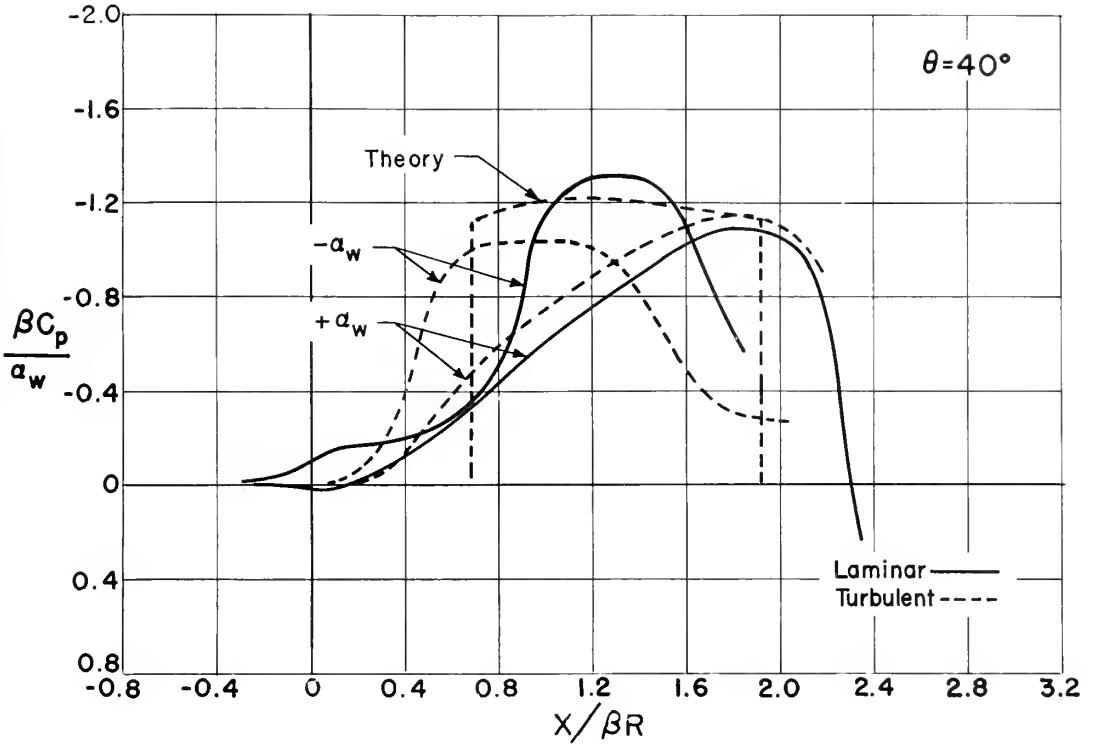

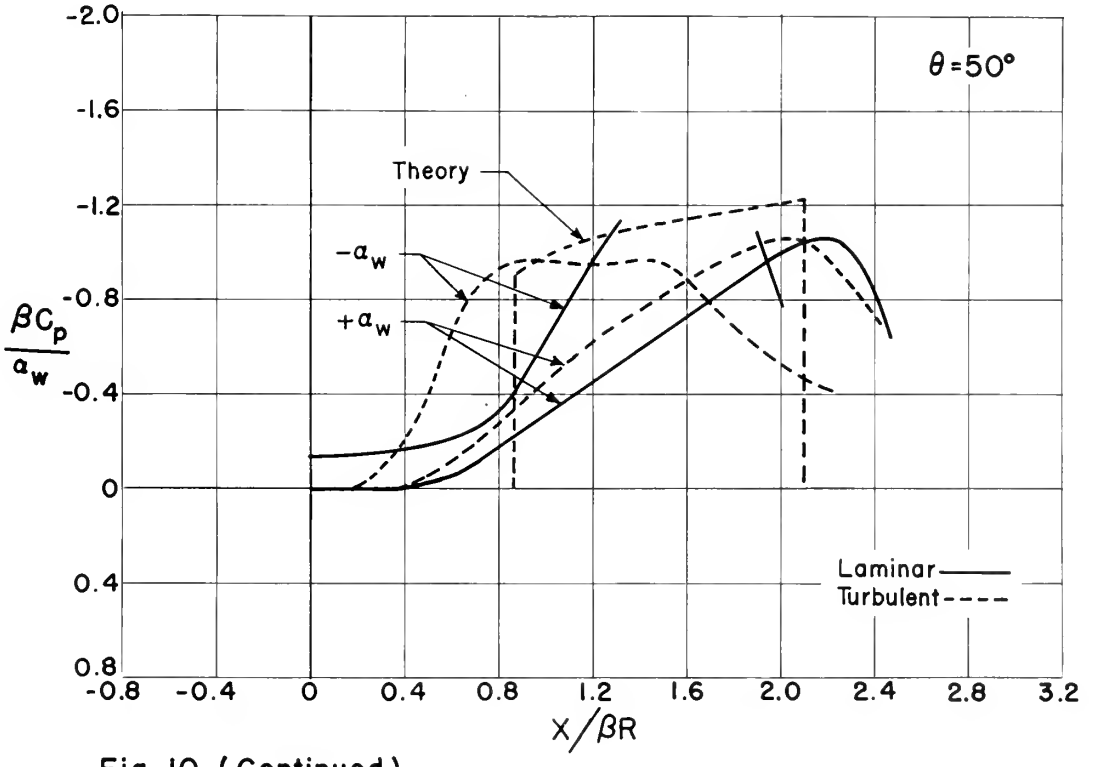

Fig. 10 (Continued)

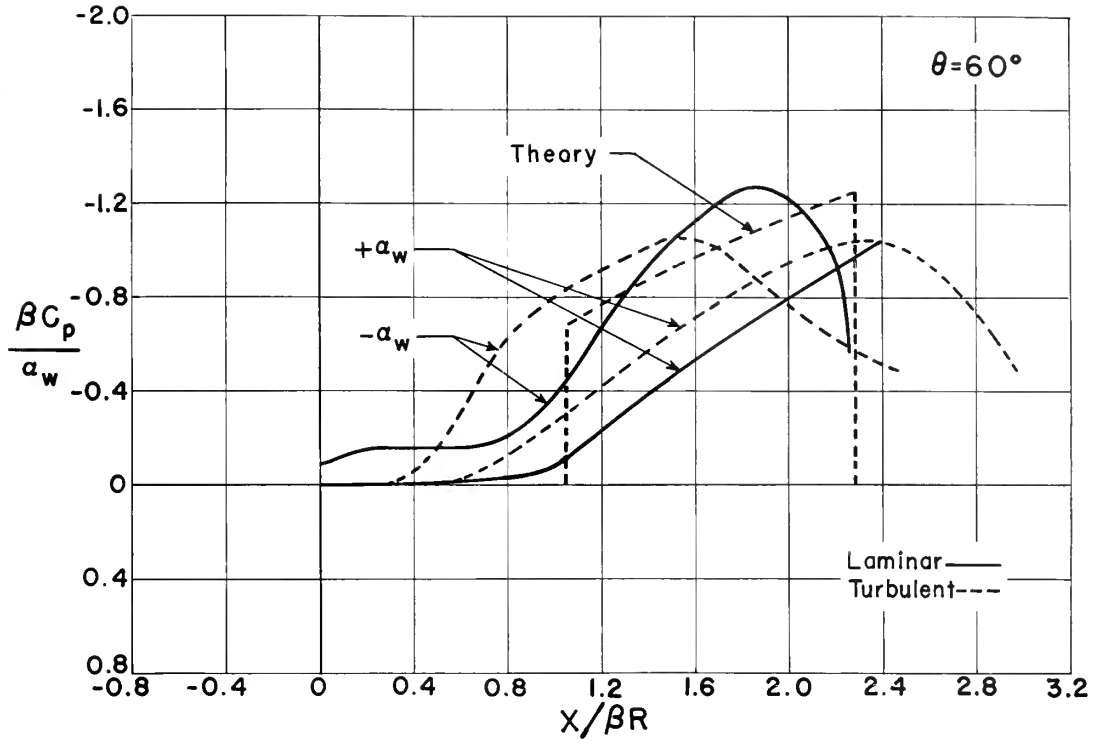

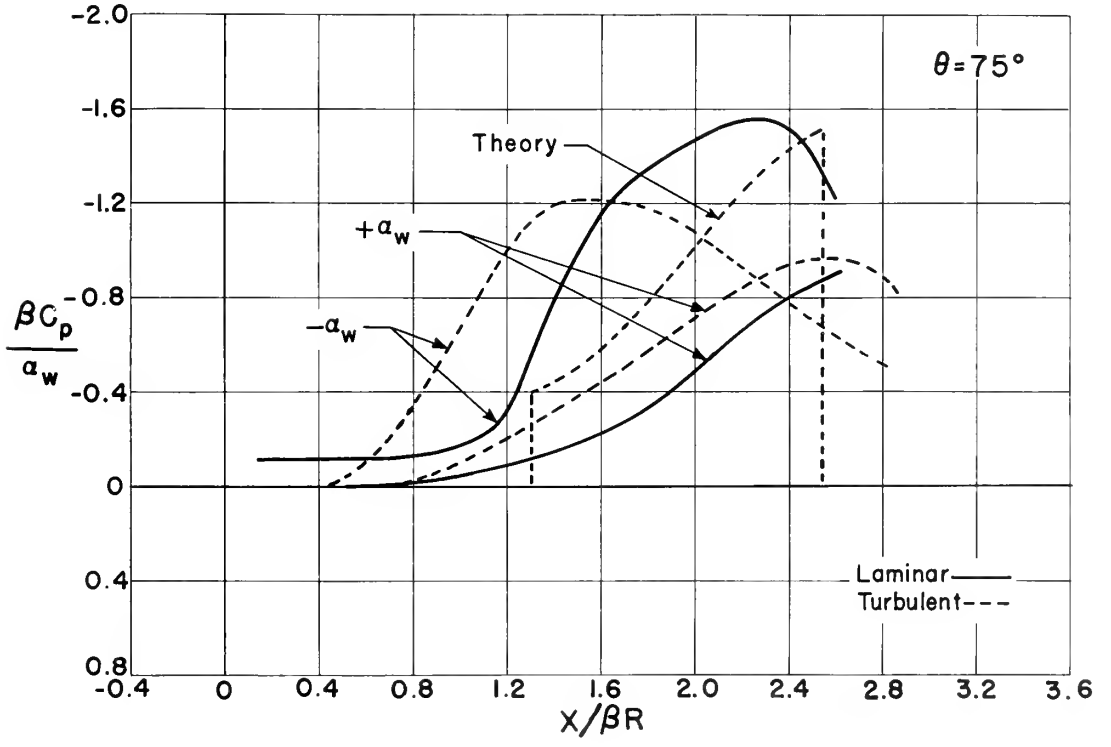

Fig. 10 (Continued)

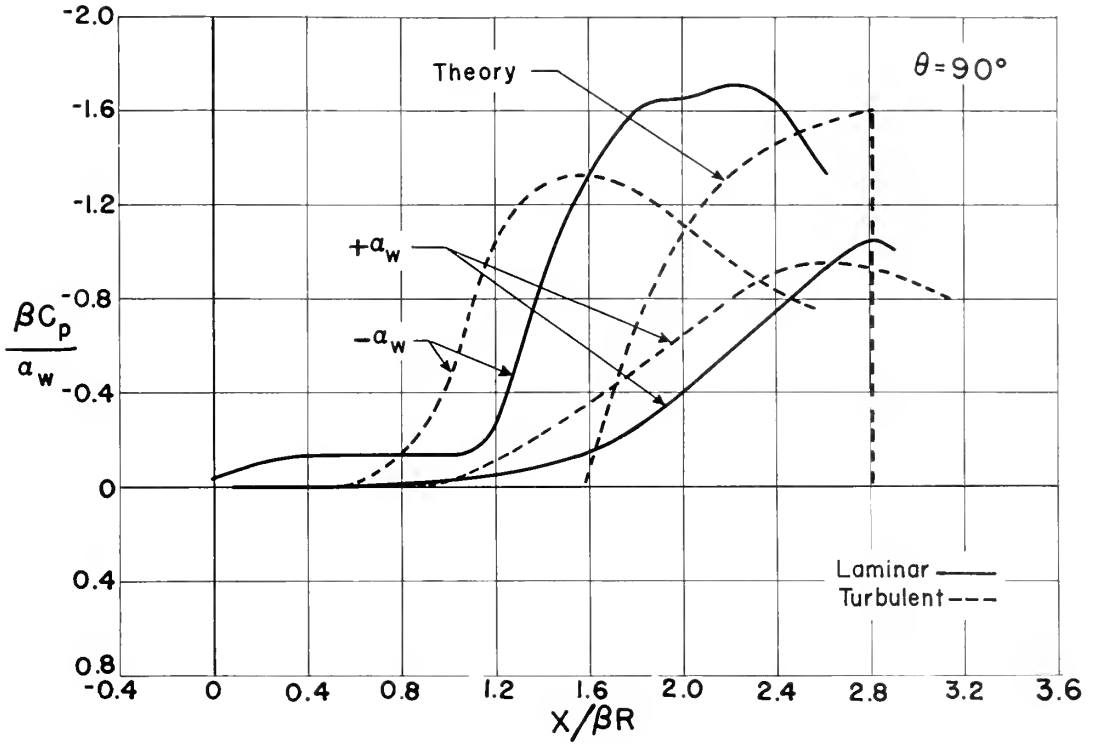

Fig. 10 (Concluded)

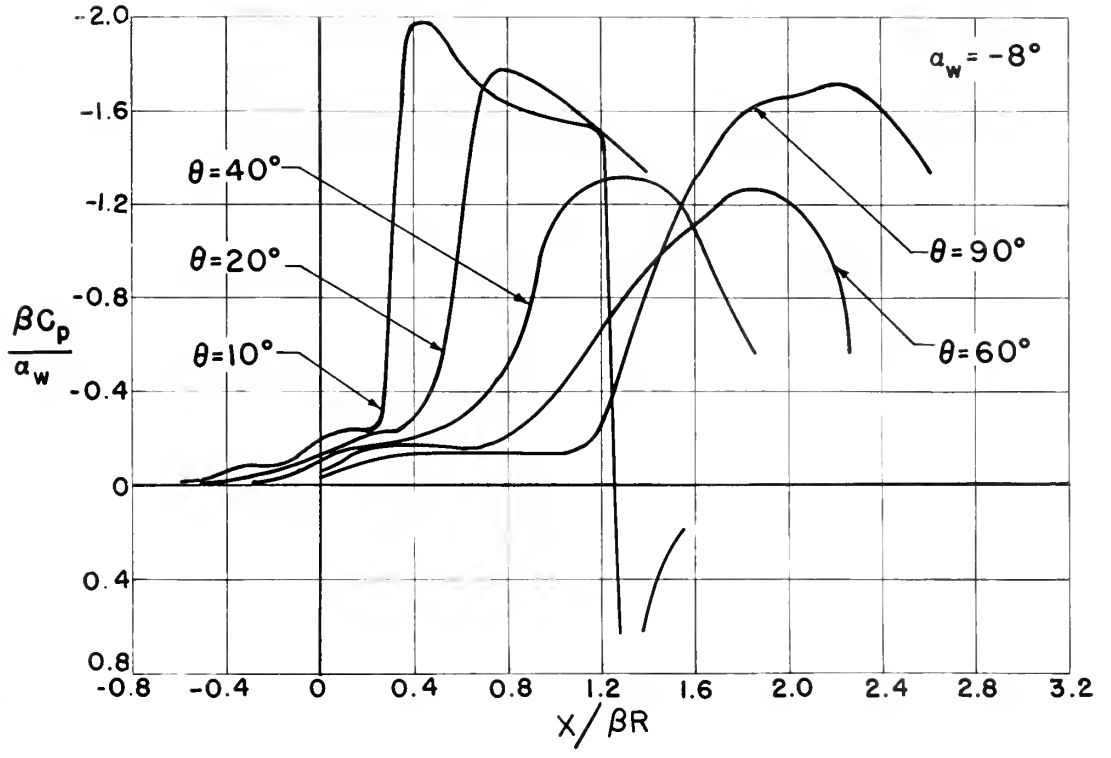

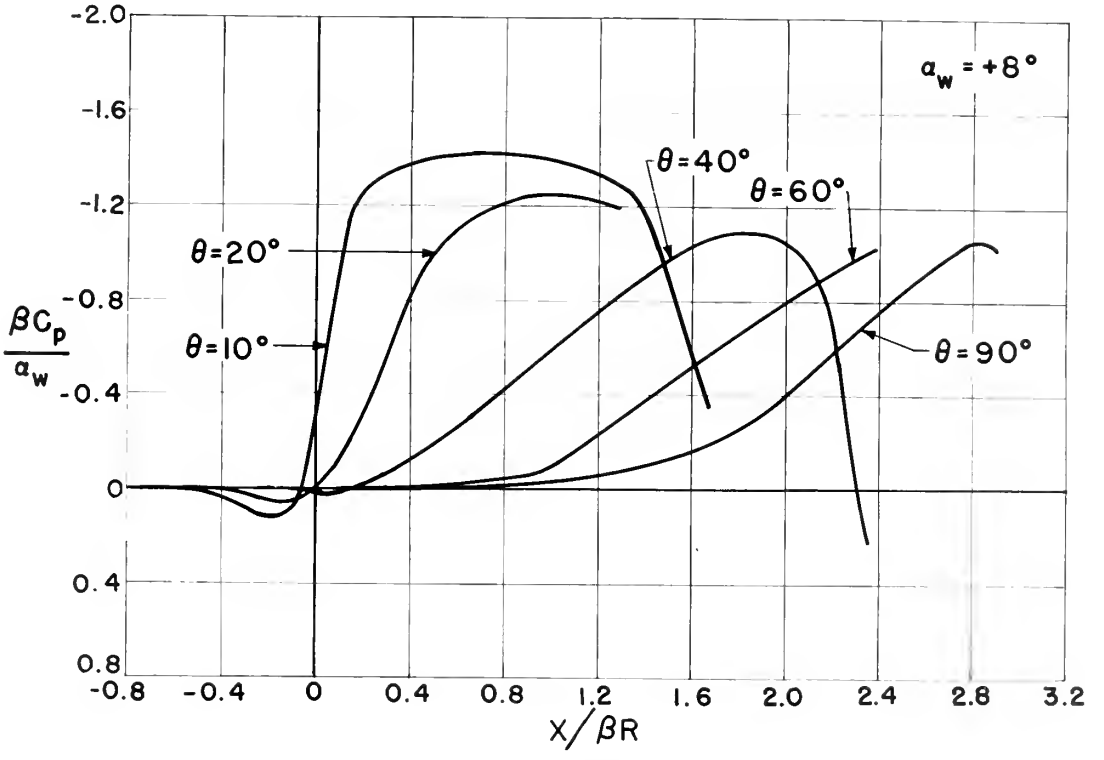

Fig. 11 Composite Pressure Profiles, $\alpha_B = 0$